Supporting Information

Heteroleptic "open ruthenocene" for deposition of Ru films from the gas phase

Roman Kultyshev*, Ian Harkness, Daniel B. G. Berry, Hoi Jobson, Huw Marchbank, Tugce Eralp Erden and Laura Ashfield

Johnson Matthey Technology Centre, Blounts Court Road, Sonning Common, Reading, RG4 9NH

*roman.kultyshev@matthey.com

Table of contents:

General information.

Synthesis. All synthetic operations were performed in an Ar glove box (MBraun Labmaster) unless stated otherwise. HBF_4-Et_2O in diethyl ether, sodium carbonate, anhydrous diethyl ether, acetonitrile and hexane were purchased from Sigma-Aldrich. Acetone and mesityl oxide were purchased from Thermo Scientific and distilled from Drierite™ and molecular sieves (3Å), respectively. Compounds (η^5-2,4-$Me_2C_5H_5)_2Ru$ (**1**) and $[(CH_3CN)_3Ru(\eta^5$-2,4-$Me_2C_5H_5)]BF_4$ (**4**) were prepared according to the published procedures.[1,2]

NMR spectra were acquired using Bruker Ultrashield™ 400 MHz spectrometer equipped with a NEO console and a 5 mm BBO BBF-H-D probe and referenced to TMS using residual non-deuterated or partially deuterated solvent signals.

Single crystal X-ray diffraction. A crystalline sample of **3**, which had been recrystallised from hexane, was isolated and suspended in oil. A suitable orange block-shaped crystal with dimensions 0.23 × 0.14 × 0.06 mm^3 was selected. This crystal was mounted on a MITIGEN holder in oil on a Rigaku FRE+ diffractometer with Arc Sec VHF Varimax confocal mirrors, a UG2 goniometer and HyPix 6000HE detector. The crystal was kept at a steady T = 100(2) K during data collection. The structure was solved with the ShelXT 2014/5 solution program[3] using dual methods and by using Olex2 1.5 as the graphical interface.[4] The model was refined with ShelXL 2014/7 (Sheldrick, 2015) using full matrix least squares minimisation on F^2.[5]

Grazing incidence angle X-ray diffraction (GI-XRD). Analysis was carried out using Bruker D8 Advance Davinci design diffractometer (Cu Kα radiation; λ = 1.54056 + 1.54439 Å). Grazing incidence angle and penetration depth were 0.5° and 66 nm, respectively. Phase identification was done using Bruker AXS Diffrac Eva V5 software (2010-2018) and PDF-4+ database (2020 release).

Film thickness and resistivity. The film thickness was measured using a FISCHERSCOPE™ X-RAY XDV™-SDD from Fischer. Film resistivity was measured by a four-point probe method using a Loresta-GX from Nittoseiko Analytech.

X-ray photoelectron spectroscopy (XPS). XPS measurements were carried out on a Thermo Scientific NEXSA with a monochromated AlKα source with a 400 μm elliptical X-ray spot. A dual beam flood gun was used for charge compensation and a pass energy of 30 eV was used. Experiments were carried out under UHV with a base pressure better than 2×10^{-9} mbar.

Preparation of (η^5-2,4-dimethylpentadienyl) tris(acetonitrile) ruthenium (II) tetrafluoroborate (4).

Compound **2** (2.9 g; 9.95 mmol) was dissolved in 126 mL diethyl ether with stirring. Within 10 min, (1.50 mL; 10.9 mmol) was added dropwise causing precipitation of a pale-yellow solid. The mixture was filtered in the glove box. The solid on the frit was washed with two 40 mL portions of ether. The solid was pumped on for 20 min (house vacuum) to remove the solvent. Most of the solid was scraped out of the filtration funnel and weighed: 3.406 g. The solid was placed into a 100 mL Schlenk flask, which was then attached to the receiving end of the filtration funnel. The funnel was capped with a rubber septum followed by addition of 25 mL acetonitrile above the frit to rinse the remaining pale-yellow solid, which dissolved immediately. The solution was filtered into the 100 mL Schlenk flask. The frit was rinsed with extra 25 mL acetonitrile. The combined filtrate was stirred briefly in the 100 mL flask, after which it was stoppered with a rubber septum

and removed from the glove box. Volatiles were removed by pumping on the stirred solution through a cold trap. The flask containing orange solid was isolated and returned to the glove box. Most of the orange solid was scraped out and weighed: 3.693 g; 96% yield.

Preparation of (η^5-2,4-dimethylpentadienyl)(η^5-2,4-dimethyl-1-oxapentadienyl)Ru (3).

A 100 mL Schlenk flask equipped with a stir bar was charged with **4** (3.257 g; 8.02 mmol). The flask was stoppered with a rubber septum followed by addition of 45 mL anhydrous acetone and stirring. With stirring, mesityl oxide (9.20 mL; 7.89 g; 80.4 mmol) was added followed by anhydrous sodium carbonate (4.250 g; 40.10 mmol) via a funnel followed by a 13 mL acetone rinse. The flask was capped and stirred overnight in the glovebox. A filtration apparatus was fitted to the flask consisting of a 200 mL filtration flask and a 200 mL Schlenk receiving flask with a stir bar. The apparatus was upended, filtration was assisted by house vacuum. The reaction flask and ppt on the frit were rinsed with 35 mL acetone to wash out the orange colour. The rinse was collected in the same receiving flask as the filtrate. The flask was disconnected, stoppered and removed from the box. The solution was pumped on through a cold trap with stirring (warm water bath) for 2 h. The flask was isolated and returned to the glove box. Hexane (50 mL) was added to the flask followed by stirring for ~2 h. The funnel was fitted with a new 200 mL Schlenk receiving flask with a stir bar. These were fitted on top of the 200 mL flask with the hexane extract. The apparatus was upended followed by filtration assisted by house vacuum. Hexane (25 mL) was added to the extracted residue in the 200 mL flask followed by shaking. This resulted in pale-yellow colour of the supernatant. The mixture was filtered using the same filtration apparatus (the second hexane extract was combined with the first). The 200 mL flask containing the hexane extract was disconnected, stoppered and removed from the glove box. The flask was pumped on through a cold trap with stirring (warm water bath) for 1 h. The flask containing an oily residue was isolated and returned to the glove box. The residue partially crystallized overnight. The flask was removed from the glove box and pumped on through a cold trap with stirring for 5 h. The flask containing a crystalline material was isolated and returned to the glove box. The crude product was scraped out and placed in a 100 mL Schlenk flask equipped with a stir bar followed by dissolution in 20 mL dry hexane. The flask was placed in a -20 ^{o}C freezer overnight. After crystallisation, the flask was removed from the freezer, and the supernatant withdrawn quickly through the rubber septum using a syringe with a stainless-steel needle. The flask was removed from the box and pumped on through a cold trap for 1 h to remove traces of hexane. The flask was returned to the glove box where the crystals of **3** were taken out and weighed: 1.604 g. Theor. yield: 2.353 g. Yield: 68.2%. ^{1}H NMR (400.232 MHz; toluene-d_8; -20 ^{o}C): δ 5.10 (s, 1H), 4.48 (s, 1H), 4.18 (s, 1H), 3.61 (d, J = 3.0 Hz, 1H), 3.03 (s, 1H), 1.97 (s, 3H), 1.71 (s, 3H), 1.44 (s, 6H), 1.25 (d, J = 3.0 Hz, 1H), 1.07 (s, 1H), -0.10 (s, 1H). ^{13}C{^{1}H} (100.648 MHz; toluene-d_8; -19 ^{o}C): δ 141.60, 109.77, 107.11, 99.22, 90.06, 87.16, 52.96, 45.12, 43.86, 27.93, 25.71, 25.52, 25.00. ^{1}H NMR (400.232 MHz; toluene-d_8; -59 ^{o}C): major rotamer (set A) δ 4.97 (s, 1H), 4.60 (s, 1H), 4.01 (s, 1H), 3.78 (br s, 1H), 3.14 (s, 1H), 1.93 (s, 3H), 1.75 (s, 3H), 1.41 (s, 3H), 1.37 (s, 1H), 1.36 (s, 3H), 1.08 (br s, 1H), -0.07 (br s, 1H). Minor rotamer (set B) δ 3.97 (s, 1H), 3.34 (s, 1H), 2.64 (s, 1H), 2.58 (br s, 1H), 2.37 (s, 1H), 1.89 (s, 3H), 1.59 (s, 1H), 1.555 (s, 3H), 1.550 (s, 3H), 0.63 (s, 1H), 0.39 (s, 1H).

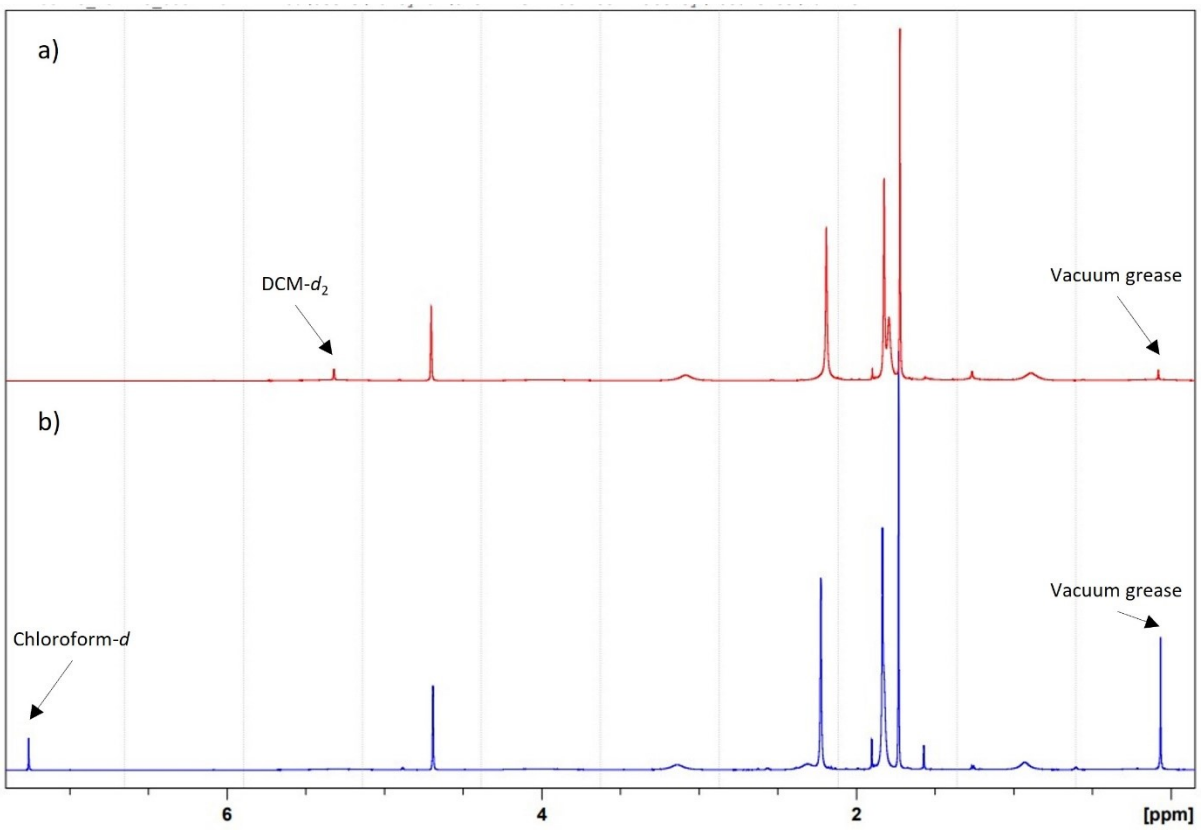

*Figure S1. Room temperature (25 °C) ^{1}H NMR spectra of **3** in a) DCM-d_2 and b) chloroform-d.*

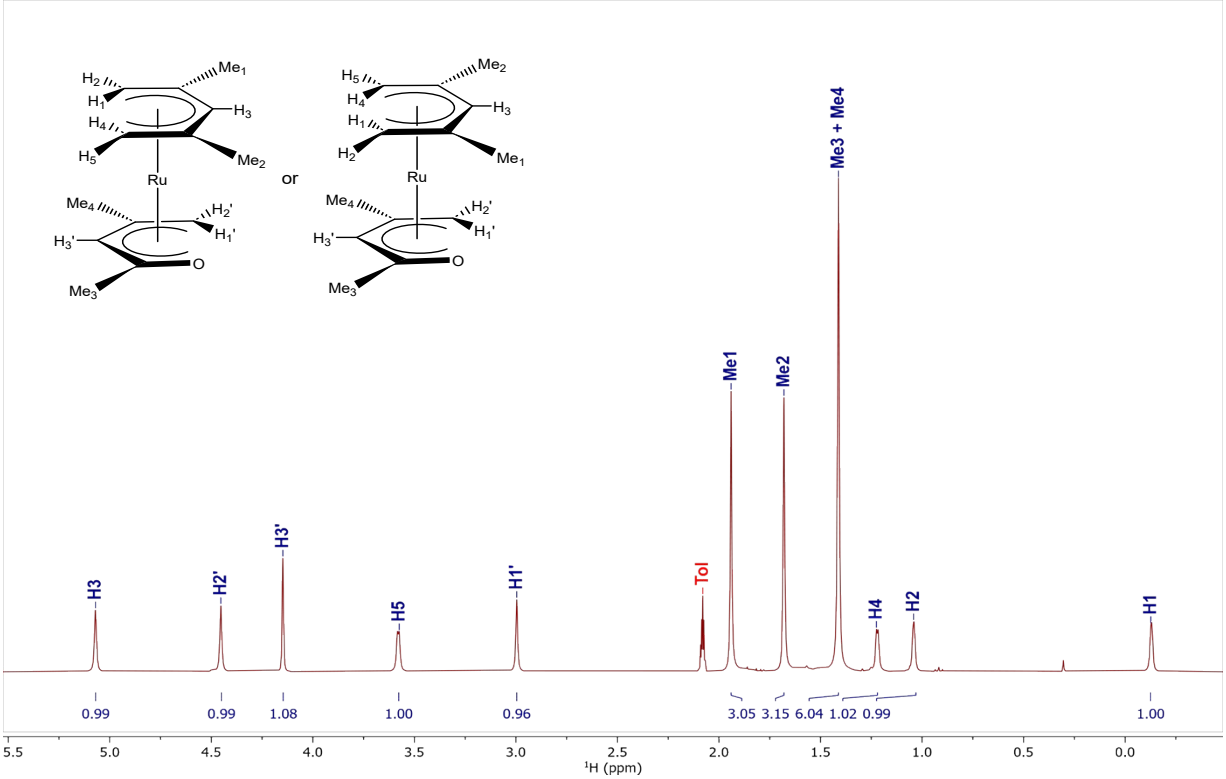

*Figure S2. ^{1}H NMR spectrum of **3** in toluene-d_8 at -20 °C with signal assignments. Please note that the relative position of η^5-2,4-$Me_2C_5H_5$ ligand with respect to the rest of the molecule could not be decided unambiguously; therefore, both possible structures are shown. The anti-conformations were chosen for simplicity of representation and are not implied.*

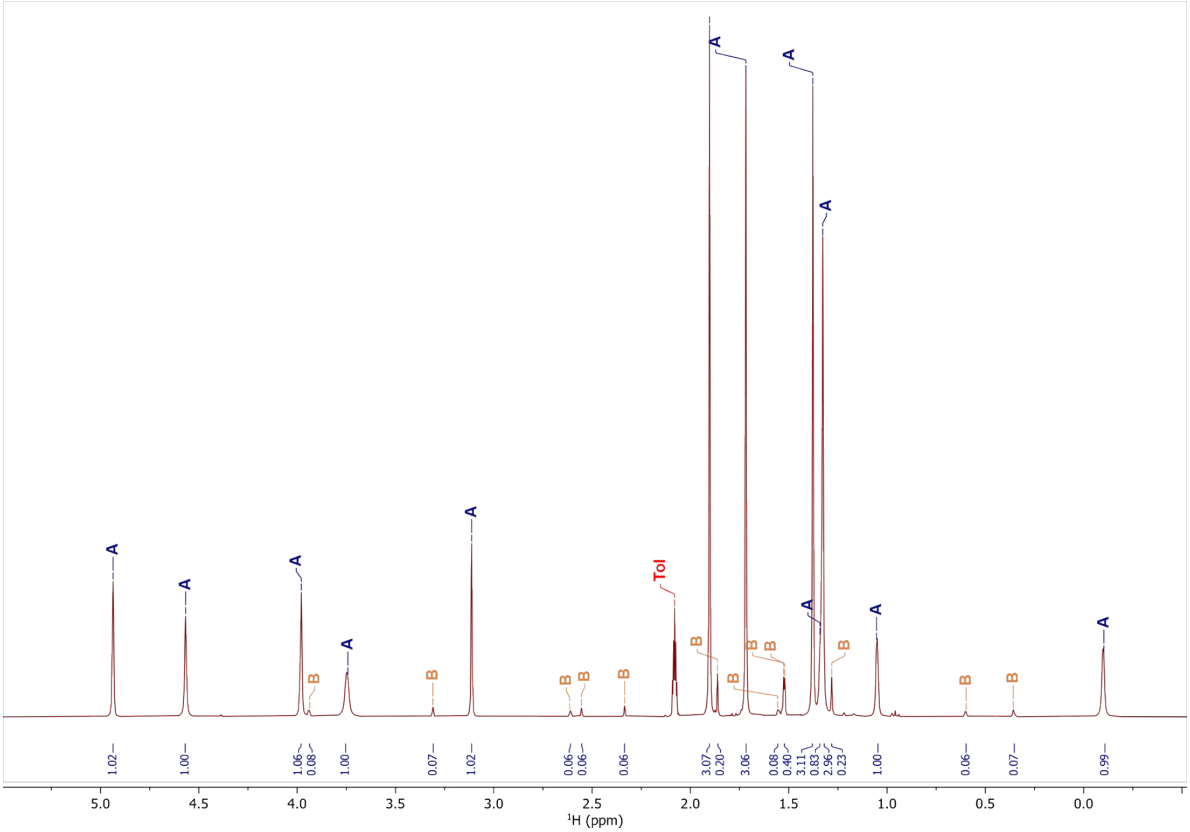

*Figure S3. ^{1}H NMR spectrum of **3** in toluene-d_8 at -60 ^{o}C with two sets of signals attributed to proposed structures for major (A) and minor (B) rotamers (see Figure S4).*

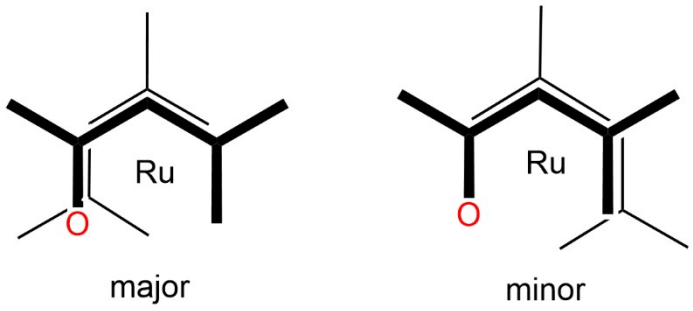

*Figure S4. Proposed structures of rotamers A (major) and B (minor) observed in the ^{1}H NMR spectrum of **3** at -60 ^{o}C (top-down view).*

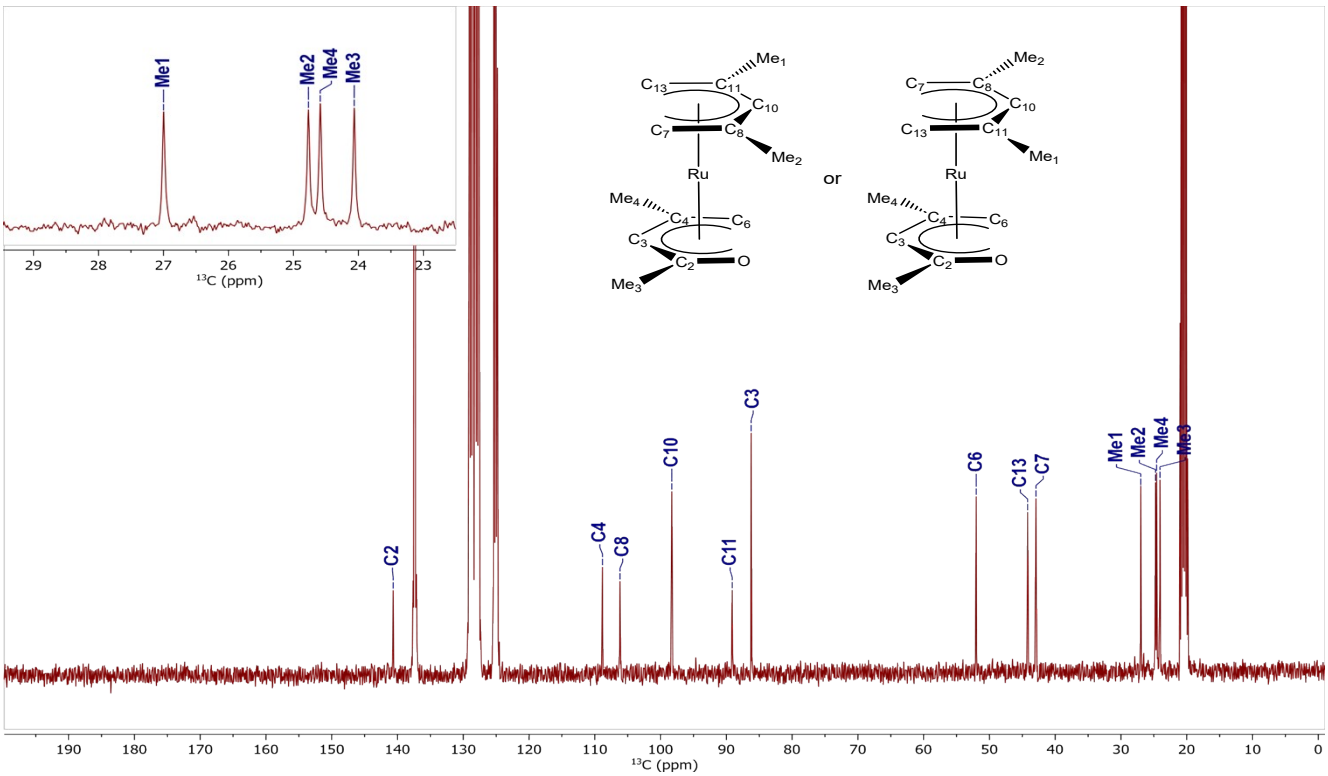

*Figure S5. $^{13}C\{^{1}H\}$ NMR spectrum of **3** in toluene-d_8 at -20 ^{o}C with signal assignments. Please note that the relative position of η^5-2,4-$Me_2C_5H_5$ ligand with respect to the rest of the molecule could not be decided unambiguously; therefore, both possible structures are shown. The anti-conformations were chosen for simplicity of representation and are not implied.*

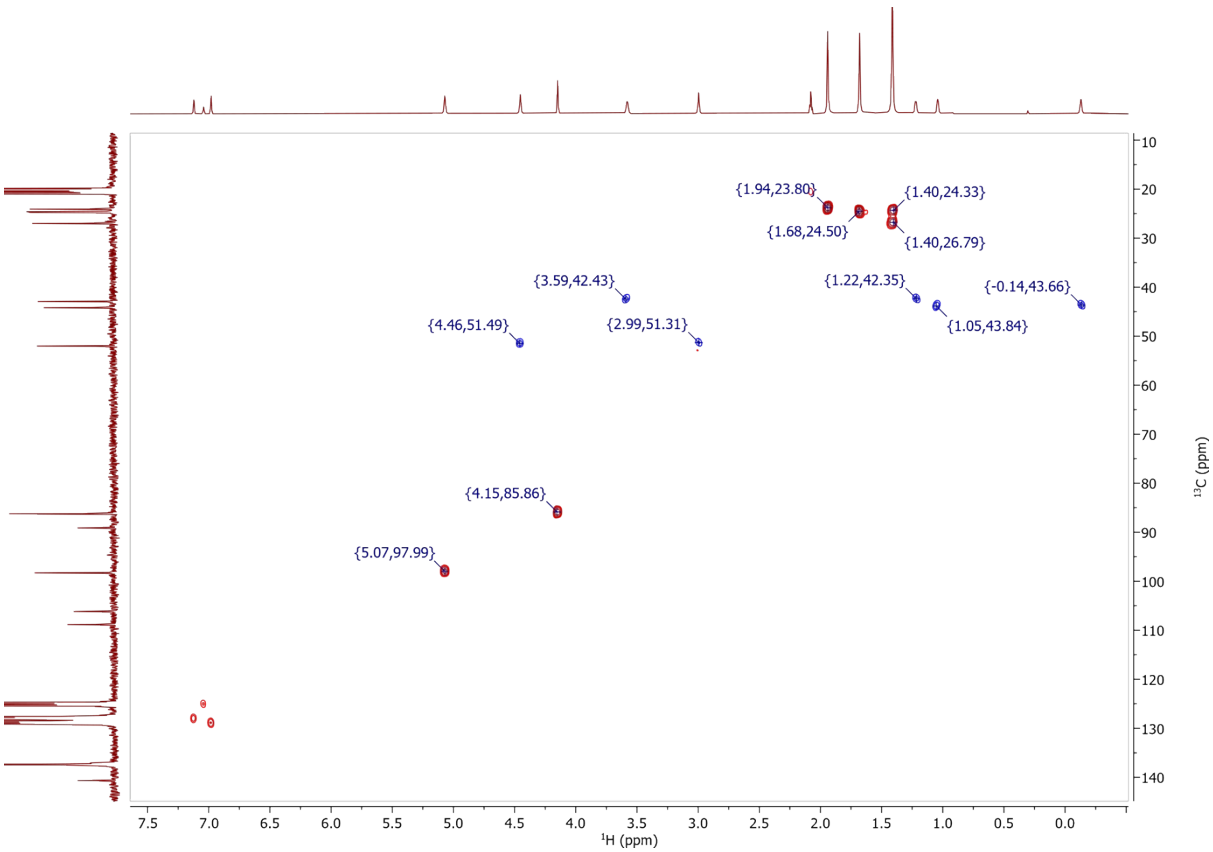

*Figure S6. ^{1}H - ^{13}C HSQC NMR spectrum of **3** in toluene-d_8 at -20 ^{o}C.*

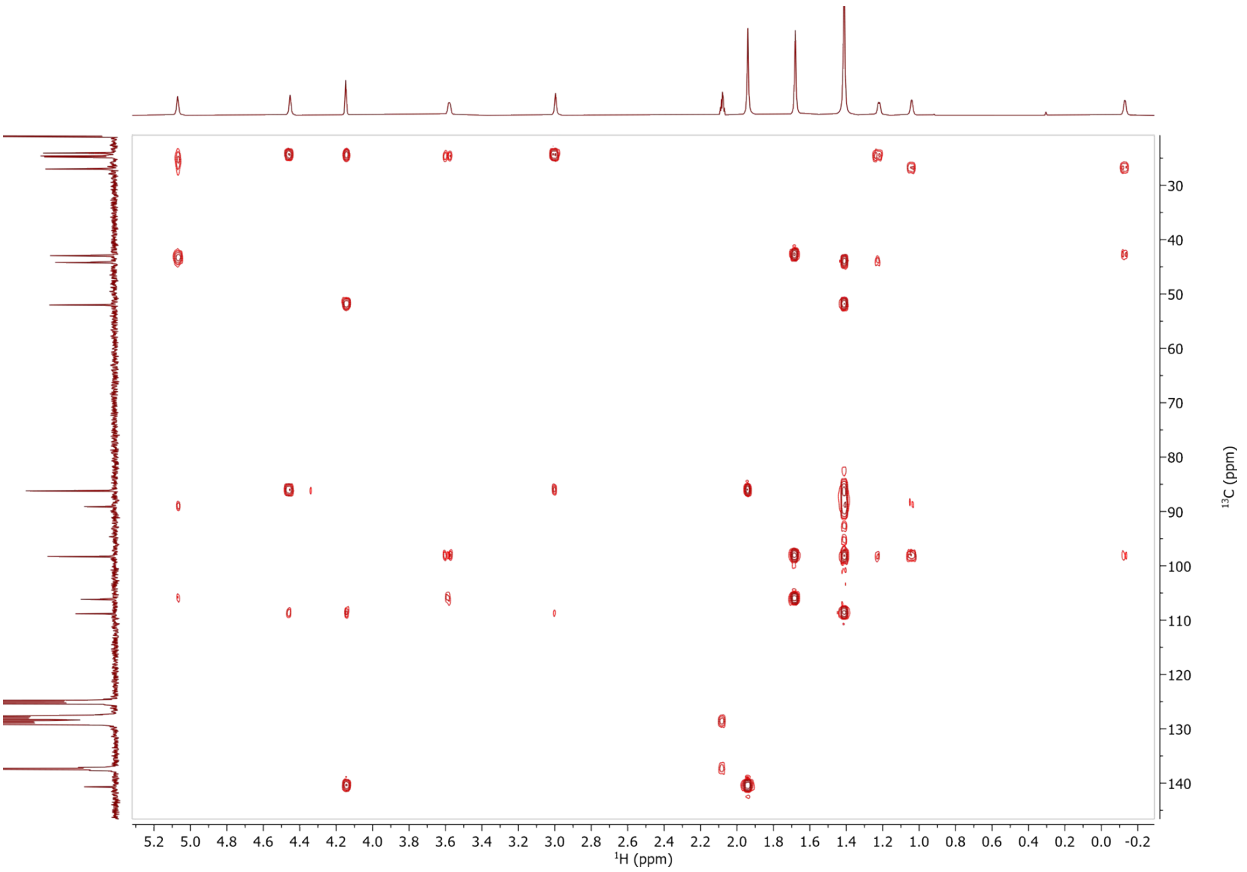

*Figure S7. ^{1}H - ^{13}C HMBC NMR spectrum of **3** in toluene-d_8 at -20 ^{o}C.*

*Table S1. Crystallographic data for **3***

Compound 3

Formula	$C_{13}H_{20}ORu$
$D_{calc.}$/ g cm^{-3}	1.573
μ/mm^{-1}	1.238
Formula Weight	293.36
Colour	orange
Shape	block-shaped
Size/mm^3	0.23×0.14×0.06
T/K	100(2)
Crystal System	monoclinic
Space Group	$P2_1/c$
a/Å	7.3396(2)
b/Å	16.8660(4)
c/Å	10.2918(3)
α/°	90
β/°	103.493(2)
γ/°	90
V/Å^3	1238.85(6)
Z	4
Z'	1
Wavelength/Å	0.71073
Radiation type	Mo K_α
Θ_{min}/°	2.366
Θ_{max}/°	29.573
Measured Refl's.	24849
Indep't Refl's	3462
Refl's I≥2 σ(I)	3152
R_{int}	0.0394
Parameters	140
Restraints	0
Largest Peak	0.487
Deepest Hole	-0.494
GooF	1.062
wR_2 (all data)	0.0529
wR_2	0.0514
R_1 (all data)	0.0233
R_1	0.0200

*Table S2. Fractional atomic coordinates (×10^4) and equivalent isotropic displacement parameters (Å^2×10^3) for **3**. U_{eq} is defined as 1/3 of the trace of the orthogonalised U_{ij}.*

Atom	x	y	z	U_{eq}
Ru1	6574.8(2)	3711.3(2)	1896.8(2)	11.67(5)
O1	8161.1(17)	2840.6(7)	1065.2(12)	21.6(2)
C1	10190(3)	2561.8(11)	3223(2)	31.3(4)
C2	9256(2)	3119.3(10)	2141.2(17)	19.2(3)
C3	9607(2)	3956.7(10)	2272.2(16)	17.2(3)
C4	8626(2)	4538.2(9)	1381.2(16)	17.1(3)
C5	8899(3)	5393.1(10)	1800.3(19)	26.1(4)
C6	7265(2)	4339.6(10)	214.0(16)	20.7(3)
C7	5111(2)	4598.0(10)	2737.7(16)	18.8(3)
C8	5896(2)	4028.7(9)	3729.8(15)	17.1(3)
C9	7325(3)	4260.5(11)	4969.3(16)	24.0(3)
C10	5455(2)	3204.1(9)	3522.8(15)	16.7(3)
C11	4536(2)	2856.7(10)	2289.4(16)	17.4(3)
C12	4749(3)	1973.1(10)	2154.9(18)	24.5(3)
C13	3735(2)	3304.6(10)	1117.4(16)	20.1(3)

*Table S3. Anisotropic displacement parameters (×10⁴) for **3**. The anisotropic displacement factor exponent takes the form: $-2p^2[h^2a^{*2} \times U_{11} + \ldots + 2hka^* \times b^* \times U_{12}]$*

Atom	U_{11}	U_{22}	U_{33}	U_{23}	U_{13}	U_{12}
Ru1	12.02(7)	11.91(7)	11.33(7)	0.06(4)	3.20(4)	0.00(4)
O1	23.9(6)	18.3(6)	25.8(6)	-5.8(5)	12.5(5)	-0.7(4)
C1	23.4(9)	26.8(9)	44.6(11)	12.9(8)	9.7(8)	10.5(7)
C2	15.2(7)	18.1(7)	26.4(8)	1.7(6)	9.2(6)	3.9(6)
C3	13.5(7)	19.8(7)	18.7(7)	-1.1(6)	4.6(5)	-2.1(6)
C4	17.5(7)	15.9(7)	20.6(7)	0.6(6)	9.7(6)	-2.1(5)
C5	29.8(9)	16.4(8)	35.5(10)	-0.6(7)	14.3(7)	-5.1(7)
C6	21.4(8)	26.1(8)	16.0(7)	4.8(6)	7.4(6)	-0.8(6)
C7	21.3(7)	16.7(7)	20.9(7)	1.6(6)	10.1(6)	4.5(6)
C8	20.2(7)	17.7(7)	15.5(7)	-1.2(5)	8.8(6)	0.3(6)
C9	29.9(9)	25.8(9)	16.2(7)	-4.6(6)	5.1(6)	-3.4(7)
C10	17.6(7)	17.9(7)	16.6(7)	3.0(5)	8.0(6)	0.9(5)
C11	15.8(7)	17.8(7)	20.3(7)	0.5(6)	7.9(6)	-3.6(5)
C12	30.4(9)	16.0(8)	29.1(9)	-1.2(6)	11.1(7)	-6.1(6)
C13	14.8(7)	24.4(8)	20.3(8)	0.4(6)	2.4(6)	-3.5(6)

*Table S4. Bond lengths for **3**.*

Atom	Atom	Length/Å
Ru1	O1	2.1702(11)
Ru1	C2	2.1681(15)
Ru1	C3	2.2070(15)
Ru1	C4	2.2059(15)
Ru1	C6	2.1881(15)
Ru1	C7	2.1385(15)
Ru1	C8	2.1288(15)
Ru1	C10	2.2022(14)
Ru1	C11	2.1825(15)
Ru1	C13	2.1626(15)
O1	C2	1.295(2)

Atom	Atom	Length/Å
C1	C2	1.496(2)
C2	C3	1.436(2)
C3	C4	1.419(2)
C4	C5	1.505(2)
C4	C6	1.412(2)
C7	C8	1.422(2)
C8	C9	1.502(2)
C8	C10	1.433(2)
C10	C11	1.418(2)
C11	C12	1.508(2)
C11	C13	1.428(2)

*Table S5. Bond angles for **3**.*

Atom	Atom	Atom	Angle/°
O1	Ru1	C3	65.43(5)
O1	Ru1	C4	82.76(5)

Atom	Atom	Atom	Angle/°
O1	Ru1	C6	76.76(6)
O1	Ru1	C10	111.50(5)

Atom	Atom	Atom	Angle/°
O1	Ru1	C11	94.60(5)
C2	Ru1	O1	34.74(6)
C2	Ru1	C3	38.32(6)
C2	Ru1	C4	70.57(6)
C2	Ru1	C6	86.76(6)
C2	Ru1	C10	102.85(6)
C2	Ru1	C11	108.50(6)
C4	Ru1	C3	37.51(6)
C6	Ru1	C3	68.76(6)
C6	Ru1	C4	37.48(6)
C6	Ru1	C10	170.37(6)
C7	Ru1	O1	177.70(5)
C7	Ru1	C2	143.42(6)
C7	Ru1	C3	112.28(6)
C7	Ru1	C4	95.21(6)
C7	Ru1	C6	102.27(6)
C7	Ru1	C10	69.65(6)
C7	Ru1	C11	87.47(6)
C7	Ru1	C13	80.81(7)
C8	Ru1	O1	141.04(5)
C8	Ru1	C2	113.99(6)
C8	Ru1	C3	103.44(6)
C8	Ru1	C4	111.60(6)
C8	Ru1	C6	136.45(6)
C8	Ru1	C7	38.93(6)
C8	Ru1	C10	38.59(6)
C8	Ru1	C11	71.92(6)
C8	Ru1	C13	90.23(6)
C10	Ru1	C3	118.66(6)
C10	Ru1	C4	145.60(6)
C11	Ru1	C3	142.98(6)
C11	Ru1	C4	176.47(6)
C11	Ru1	C6	139.62(6)
C11	Ru1	C10	37.73(6)
C13	Ru1	O1	101.44(6)
C13	Ru1	C2	131.82(6)
C13	Ru1	C3	165.79(6)
C13	Ru1	C4	139.82(6)
C13	Ru1	C6	103.94(6)
C13	Ru1	C10	70.15(6)
C13	Ru1	C11	38.38(6)
C2	O1	Ru1	72.54(8)
O1	C2	Ru1	72.72(9)
O1	C2	C1	119.57(15)
O1	C2	C3	119.93(14)
C1	C2	Ru1	128.44(12)
C3	C2	Ru1	72.31(8)
C3	C2	C1	120.47(16)
C2	C3	Ru1	69.37(8)
C4	C3	Ru1	71.21(9)
C4	C3	C2	124.49(14)
C3	C4	Ru1	71.29(8)
C3	C4	C5	117.62(15)
C5	C4	Ru1	126.12(11)
C6	C4	Ru1	70.57(9)
C6	C4	C3	122.51(15)
C6	C4	C5	119.45(15)
C4	C6	Ru1	71.95(9)
C8	C7	Ru1	70.17(9)
C7	C8	Ru1	70.90(9)
C7	C8	C9	121.33(15)
C7	C8	C10	120.59(14)
C9	C8	Ru1	123.85(11)
C10	C8	Ru1	73.48(8)
C10	C8	C9	117.90(14)
C8	C10	Ru1	67.93(8)
C11	C10	Ru1	70.38(8)
C11	C10	C8	125.33(14)
C10	C11	Ru1	71.89(9)
C10	C11	C12	116.91(15)
C10	C11	C13	123.60(15)
C12	C11	Ru1	123.03(11)
C13	C11	Ru1	70.06(9)
C13	C11	C12	118.44(15)
C11	C13	Ru1	71.56(9)

*Table S6. Torsion angles for **3**.*

Atom	Atom	Atom	Atom	Angle/°
Ru1	O1	C2	C1	124.90(15)
Ru1	O1	C2	C3	-56.88(12)

Atom	Atom	Atom	Atom	Angle/°
Ru1	C2	C3	C4	-47.45(14)
Ru1	C3	C4	C5	121.68(13)
Ru1	C3	C4	C6	-50.78(13)
Ru1	C7	C8	C9	118.64(14)
Ru1	C7	C8	C10	-56.34(12)
Ru1	C8	C10	C11	-43.00(14)
Ru1	C10	C11	C12	118.50(13)
Ru1	C10	C11	C13	-49.59(14)
O1	C2	C3	Ru1	57.08(12)
O1	C2	C3	C4	9.6(2)
C1	C2	C3	Ru1	-124.71(15)
C1	C2	C3	C4	-172.16(15)
C2	C3	C4	Ru1	46.74(14)
C2	C3	C4	C5	168.42(14)
C2	C3	C4	C6	-4.0(2)
C3	C4	C6	Ru1	51.09(13)
C5	C4	C6	Ru1	-121.24(14)
C7	C8	C10	Ru1	55.13(12)
C7	C8	C10	C11	12.1(2)
C8	C10	C11	Ru1	42.14(14)
C8	C10	C11	C12	160.64(14)
C8	C10	C11	C13	-7.5(2)
C9	C8	C10	Ru1	-120.03(13)
C9	C8	C10	C11	-163.02(15)
C10	C11	C13	Ru1	50.34(14)
C12	C11	C13	Ru1	-117.57(14)

*Table S7. Hydrogen fractional atomic coordinates (×10⁴) and equivalent isotropic displacement parameters (Å²×10³) for **3**. U_{eq} is defined as 1/3 of the trace of the orthogonalised U_{ij}.*

Atom	x	y	z	U_{eq}
H1A	10713	2862	4040	47
H1B	11199	2278	2942	47
H1C	9269	2179	3397	47
H3	10216	4148	3191	21
H5A	7758	5693	1412	39
H5B	9952	5615	1485	39
H5C	9164	5428	2777	39
H6A	7696	4009	-450	25
H6B	6397	4769	-193	25
H7A	5674	5134	2845	23
H7B	3729	4601	2429	23
H9A	8137	3806	5292	36
H9B	6685	4426	5661	36
H9C	8084	4700	4764	36
H10	6340	2841	4131	20
H12A	5418	1864	1454	37
H12B	3508	1725	1918	37
H12C	5461	1756	3005	37
H13A	2723	3679	1186	24
H13B	3493	3014	258	24

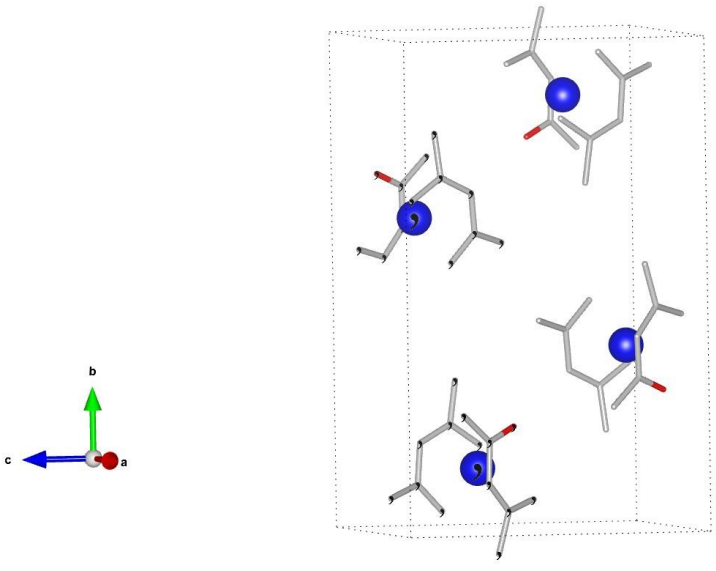

*Figure S8. $P2_1/c$ unit cell of the crystal structure of **3** showing two pairs of (R)- and (S)-enantiomers related through the centre of symmetry.*

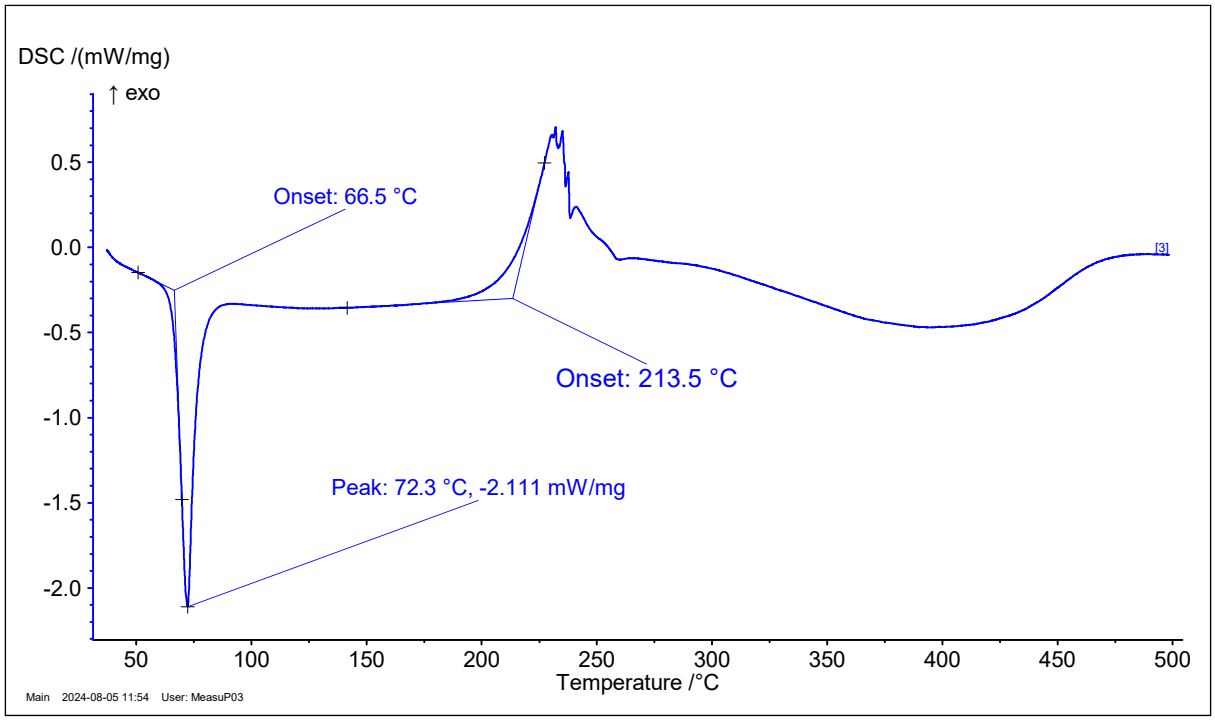

*Figure S9. Differential scanning calorimetry (DSC) trace of **3** at 10 °C /min.*

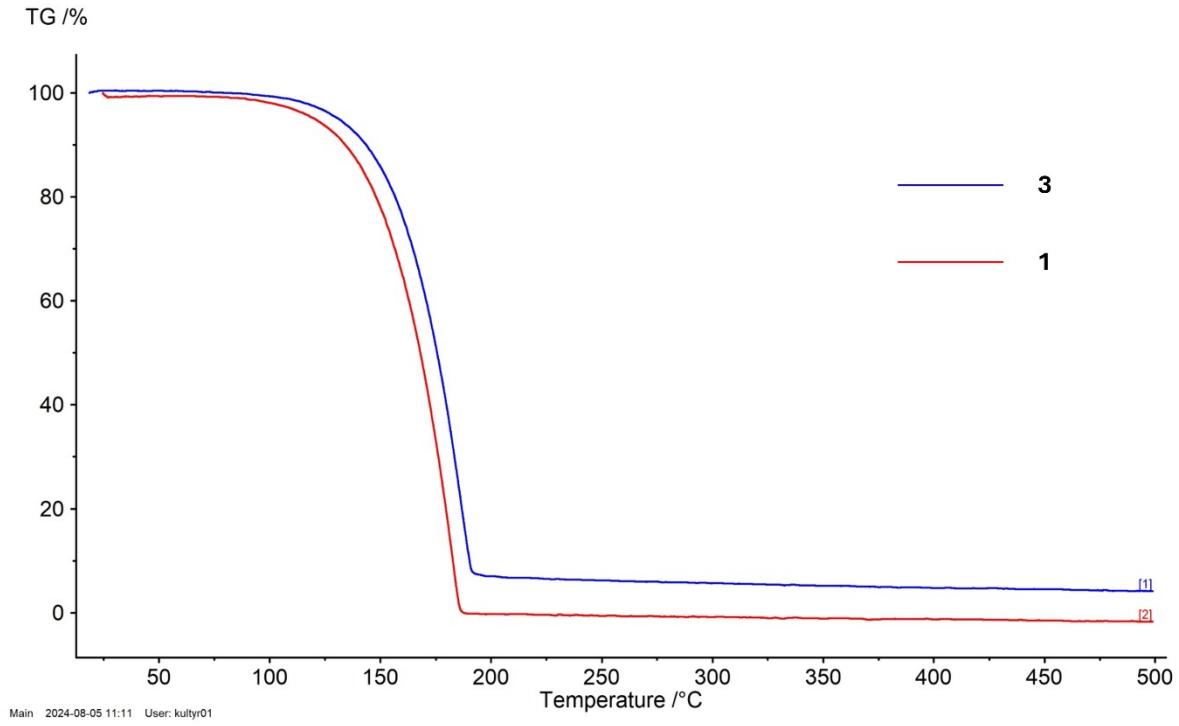

*Figure S10. Non-isothermal TGA traces of **1** and **3** between 25 and 500 °C at 5 °C/min. Experiments were run under nitrogen flow (50 mL/min).*

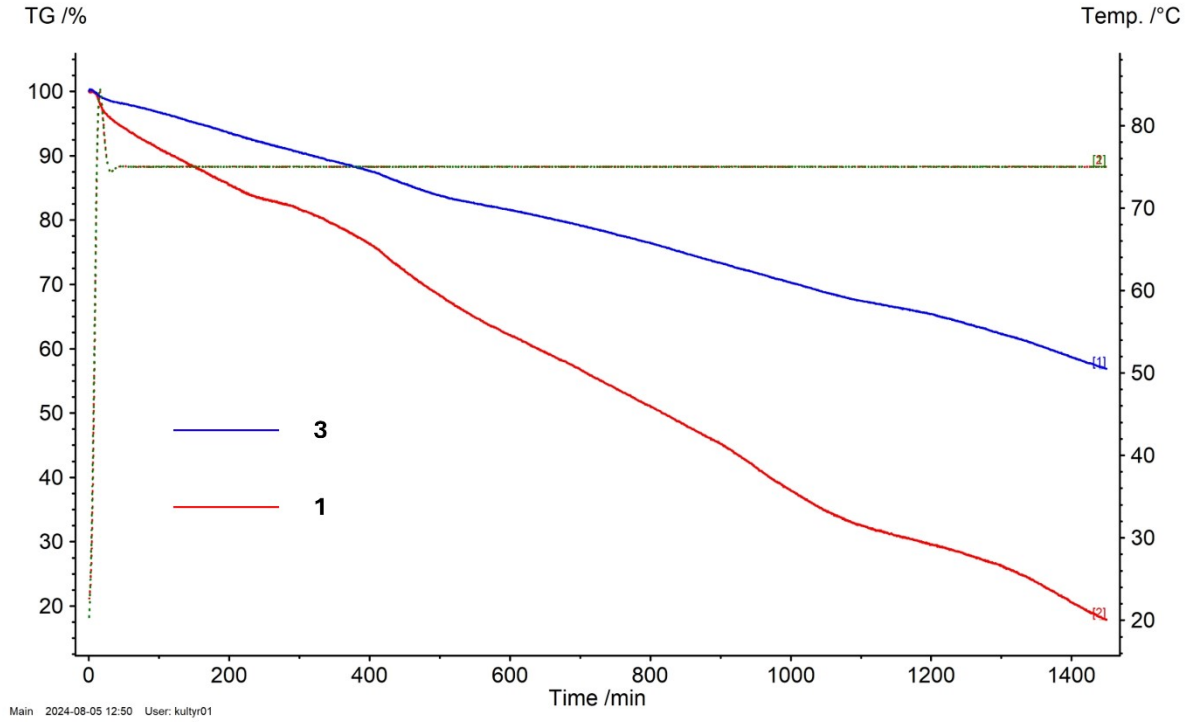

*Figure S11. Isothermal TGA traces of **1** and **3** at 75 °C (24 h). Experiments were run under nitrogen flow (50 mL/min).*

Vapour pressure determination of 3 by Knudsen effusion method.[6]

Two samples of **3** (Sample 1 – 212.3 mg and Sample 2 – 217.5 mg; both comprised **3** prepared by crystallization from hexane) were placed in alumina Knudsen cells with orifice diameters of 98 μm (Netzsch). High-temperature Apiezon H vacuum grease was applied to the rim of the lid before closing. Each closed cell was wrapped with Teflon tape to prevent the lid from moving due to the vapor pressure build-up during the experiment. The closed Knudsen cell was placed in a Netzsch STA 449 F3 Jupiter TG analyser connected to an oil pump. After the furnace was evacuated to 4×10^{-2} mbar, a TG program consisting of a series of isothermal steps was run. The measured TG curves were parsed and analysed by a Python script. A simplified Knudsen effusion equation was used to calculate the vapor pressure at a given temperature (reference):

$$P = (dm/dt)(2\pi RT/M)^{1/2}(WS)^{-1} \quad \text{(Eq. 1)}$$

where P is the vapor pressure in the cell, dm/dt is the mass loss rate of the sample, S is the orifice area, R is the gas constant, T is the absolute temperature of the sample, M is the molecular mass of the compound, and W is the Clausing factor expressed as where l is the thickness of the Knudsen cell lid,

$$W = (1 + 3l/8r)^{-1} \quad \text{(Eq. 2)}$$

and r is the radius of the orifice. The molecular mass used in the calculation of the vapor pressure of X was 293.37 Da. The sublimation enthalpy and entropy can be derived by fitting the data to the Clausius-Clapeyron equation, where A is $\Delta_{sub}H/R$ and B is $\Delta_{sub}S/R$:

$$ln\ P = -A/T + B \qquad \text{(Eq. 3)}$$

Four measurement runs were carried out to determine and confirm a reliable range for the vapor pressure. In run 1, benzoic acid was used as a reference to check the sample holder. The temperature profile to determine the vapor pressure was: 100 (2 h), 90 (2 h), 80 (2 h), 70 (2 h), 60 (2 h), and 50 °C (2 h). Data from run 1 was compared with a previous test using benzoic acid. The results were satisfactory as variation between samples was <5% for temperatures above 50 °C. In run 2, the vapor pressure of **3** was estimated in the range of 30 – 80 °C using Sample 1. The following temperature profile was used: 30 (4 h), 40 (4 h), 50 (2 h), 60 (2 h), 70 (1h), and 80 °C (1 h). When going through the isothermal steps from the lowest to the highest temperature, the apparent vapor pressure was overestimated at lower temperatures. This overestimation was most likely due to the presence of volatile impurities, such as hexane, in the sample. The data obtained from run 2 was not used in the final analysis. Sample 1 did not show a sign of degradation based on the mass-loss rate from the TGA. As starting the measurement at the highest temperature removes volatile impurities, Sample 1 was re-used in run 3, where temperature was changed from 110 °C to 50 °C in 10 deg increments, with each isothermal step lasting 2 h, except for the 50 °C one (3 h). Run 4, in which Sample 2 was used, had the same temperature profile as Run 3. The vapor pressure values calculated according to Eq. 1 based on the mass loss rates measured in the 50 – 110 °C temperature interval are shown in Table S8.

*Table S8. Vapor pressure of **3** at 50 – 110 °C obtained from the Knudsen effusion method.*

Temperature, °C	Pressure (Pa)		
	Sample 1 (Run 3)	Sample 2 (Run 4)	Mean of two runs
110	163.7	122.7	143.2
100	80.9	70.8	75.9
90	42.5	45.5	44.0
80	22.5	29.5	26.0
70	11.5	17.8	14.7
60	6	10.3	8.2
50	163.7	122.7	143.2

Fitting the mean vapor pressure data to the Clausius-Clapeyron equation resulted in the following linear dependance on temperature described by (Eq. 4), where T is in K and P is in Pa:

$$ln\ P = -6931/T + 22.88 \quad \text{(Eq. 4)}$$

From the value of coefficient A, the sublimation enthalpy ($\Delta_{sub}H$) for X in the 50 – 110 °C temperature interval could be calculated as -57.6 ± 2.7 kJ/mol·K. The linear fit of the vapor pressure data derived from the Knudsen effusion method and the calculated vapor pressure of **3** are shown in Figure S12.

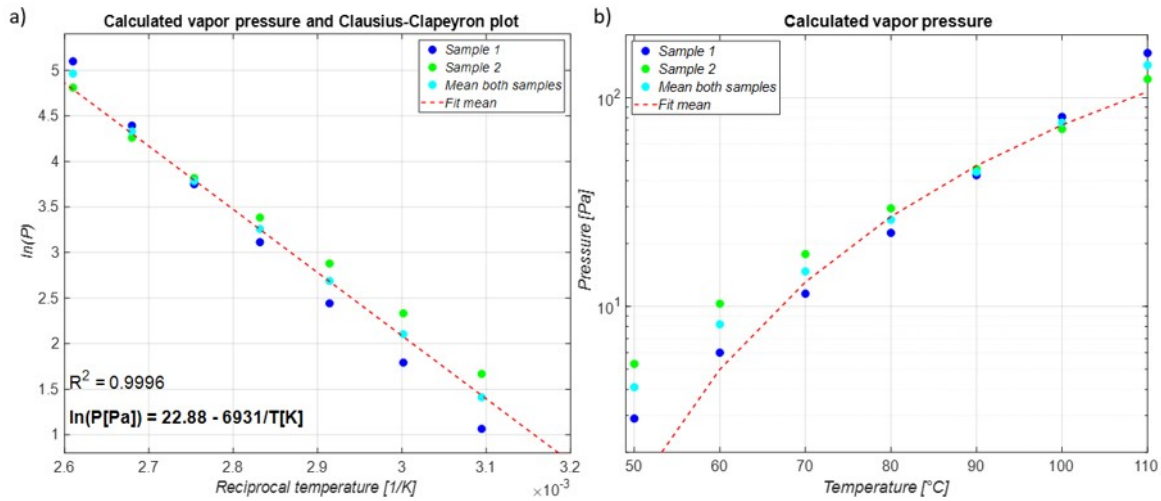

*Figure S12. (a) The linear fit of the experimental vapour pressure of **3** to Clausius-Clapeyron equation and (b) experimental vs. calculated vapor pressure dependence on temperature.*

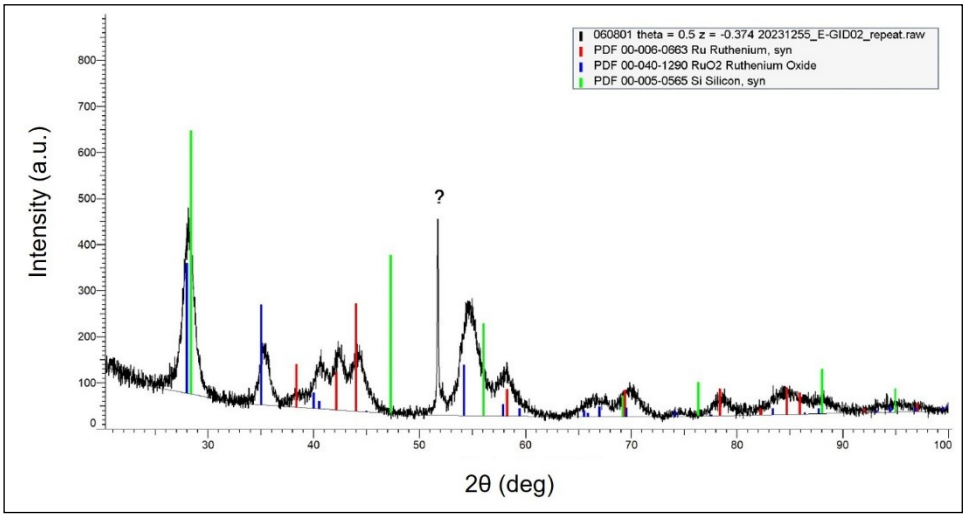

Figure S13. GI-XRD pattern of 12 nm film grown at 200 °C (in black). The peak with a question mark at 2ϑ ~ 52° has not been identified.

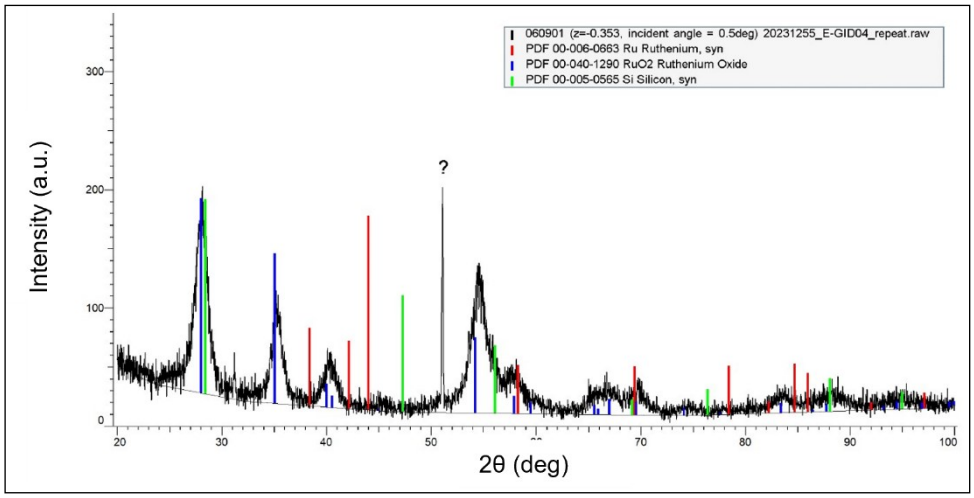

Figure S14. GI-XRD pattern of 8 nm film grown at 180 °C (in black). The peak with a question mark at 2ϑ ~ 52° has not been identified.

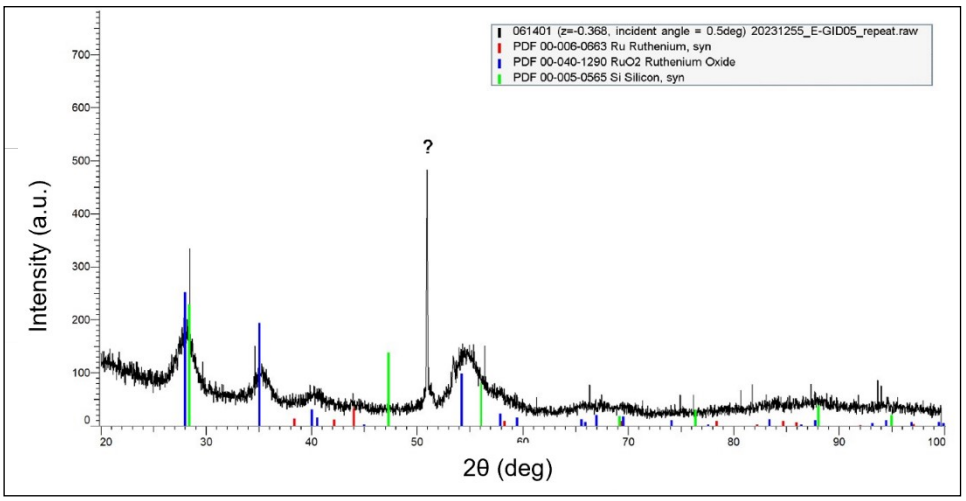

Figure S15. GI-XRD pattern of 6 nm film grown at 165 °C (in black). The peak with a question mark at 2ϑ ~ 52° has not been identified.

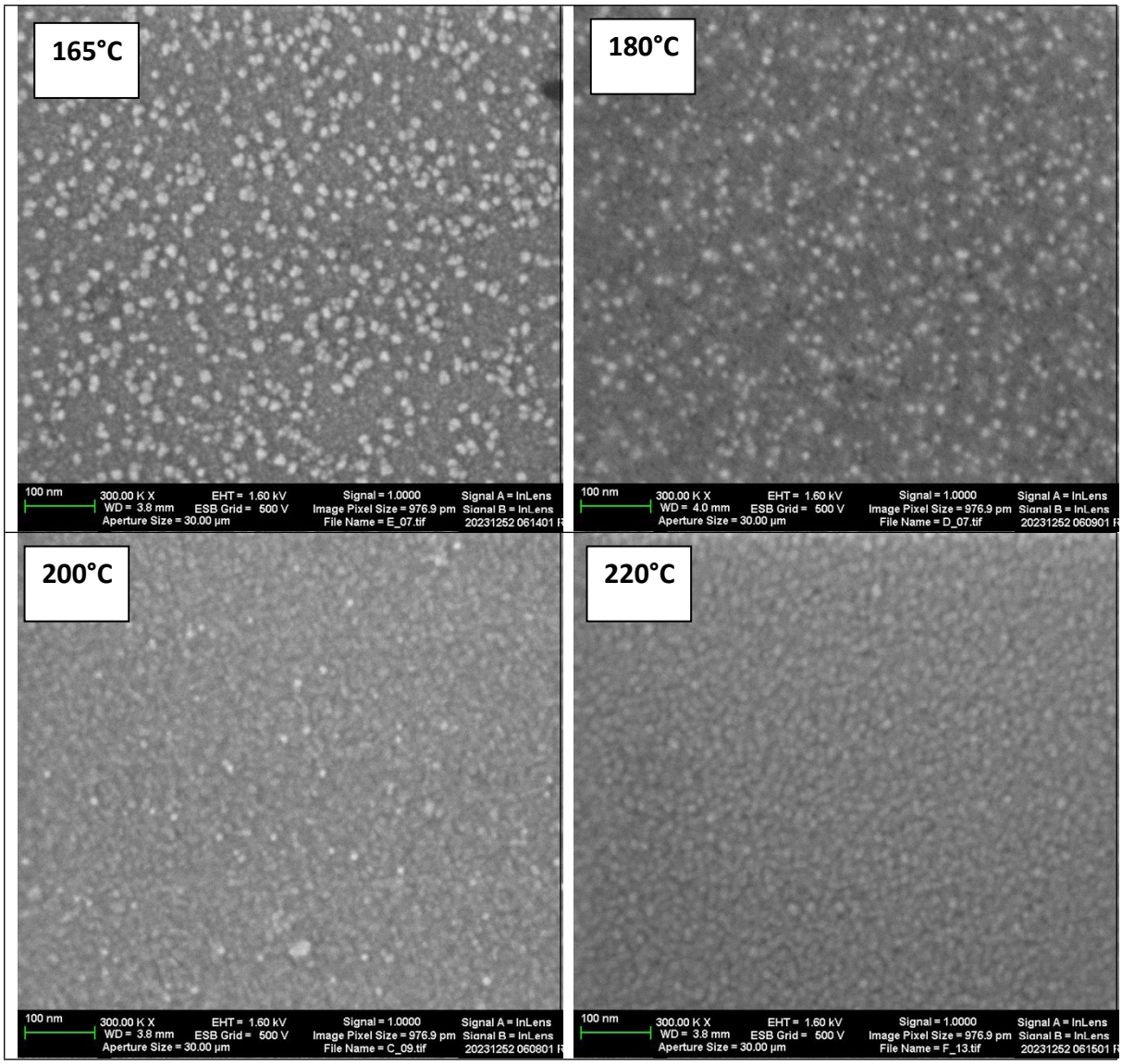

*Figure S16. Top-down SEM images (scale: 100 nm) of films deposited at different temperatures using **3**.*

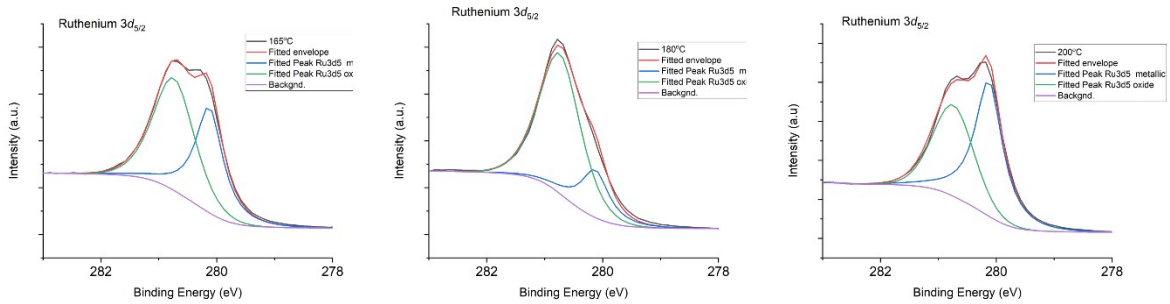

Figure S17. Fitted Ru $3d_{5/2}$ XPS of the films deposited between 165 and 200 °C.[7]

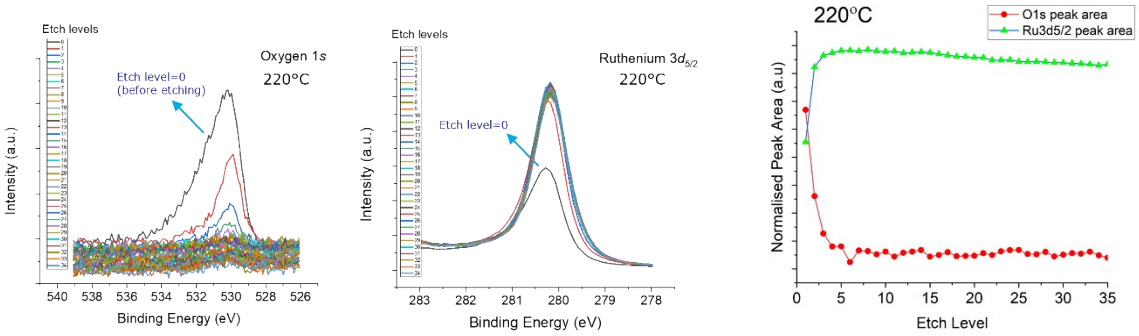

Figure S18. Oxygen 1s and ruthenium $3d_{5/2}$ spectra from Ar^+ etching experiment. Normalised peak areas are displayed over 34 etching cycles.

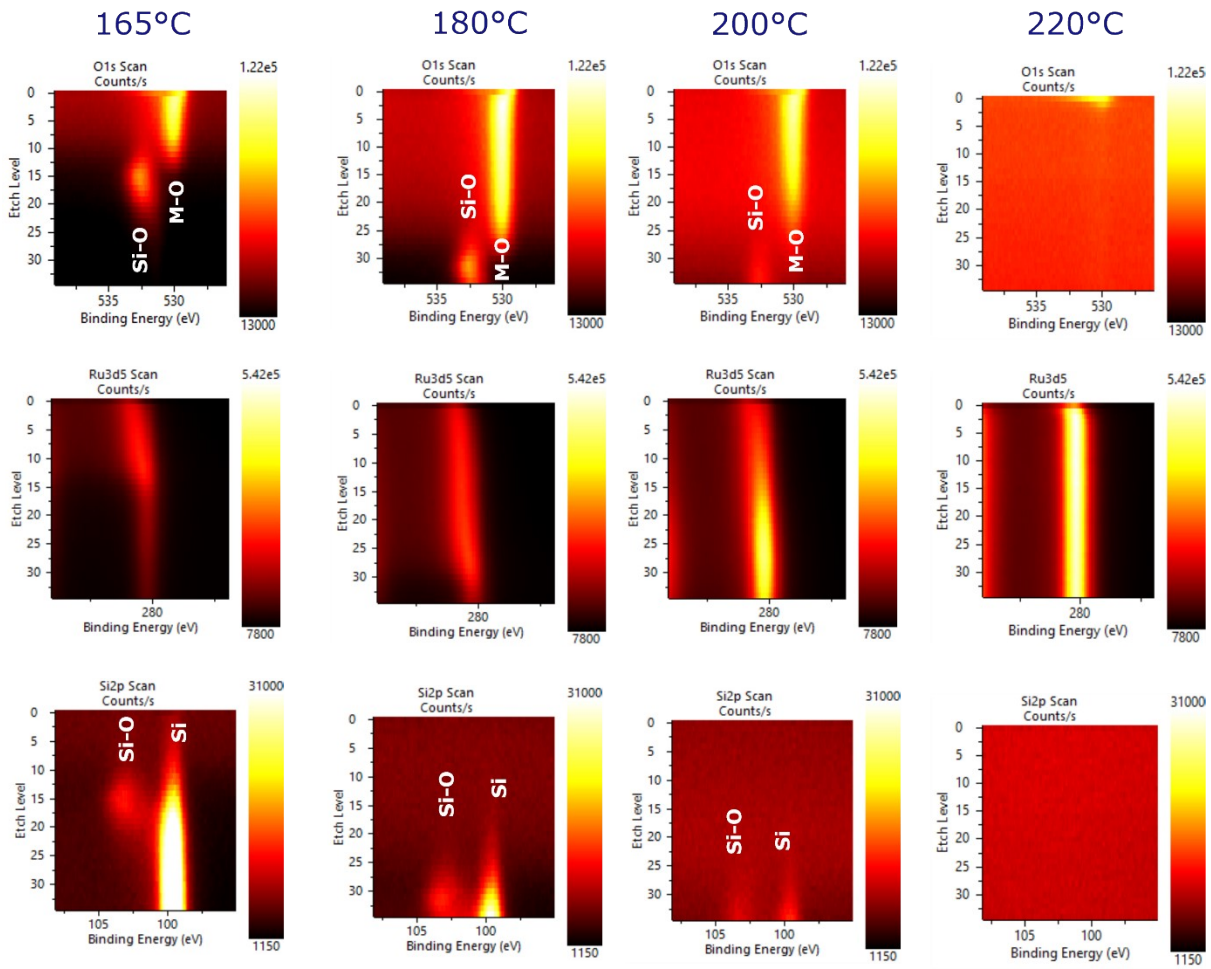

Figure S19. Waterfall intensity plots of oxygen 1s, ruthenium $3d_{5/2}$ and silicon 2p spectra over 34 Ar^+ etching cycles for the films deposited between 165 and 220 °C. Note that each line in the waterfall plot represents an oxygen 1s (or ruthenium $3d_{5/2}$) spectrum after an etching cycle.

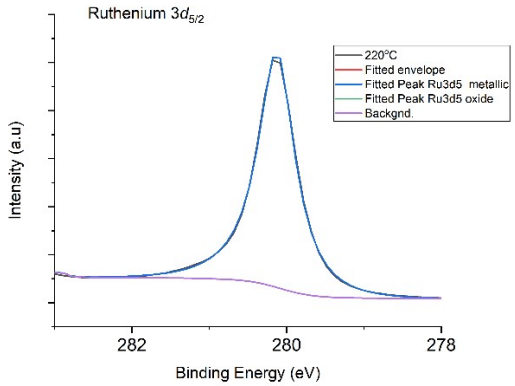

Figure S20. Fitted Ru $3d_{5/2}$ XPS of the film deposited at 220 °C.

References:

1 L. Stahl and R.D. Ernst, *Organometallics,* 1983, **2**, 1229-1234.
2 Lumini, T.; Cox, D.N.; Roulet, R.; Schenk, K. *J. Organomet Chem.* 1992, **434**, 363-385.
3 G. M. Sheldrick, *Acta Cryst*., 2015, **A71**, 3-8.
4 O.V. Dolomanov; L.J. Bourhis; R.J. Gildea; J.A.K. Howard and H. Puschmann, *J. Appl. Cryst.*, 2009, **42**, 339-341.
5 G. M. Sheldrick, *Acta Cryst*., 2015, **C71**, 3-8.
6 D. E. Kravchenko, Ph.D. Thesis, KU Leuven, 2021.
7 Y. Kotsugi, S.-M. Han, Y.-H. Kim, T. Cheon, D. K. Nandi, R. Ramesh, N.-K. Yu, K. Son, T. Tsugawa, S. Ohtake, R. Harada, Y.-B. Park, B. Shong and S.-H. Kim, *Chem. Mater.*, 2021, **33**, 5639-5651.